63-3-1

FTD-TT- 62-1644

TRANSLATION

NEWS OF SCHOOLS OF HIGHER EDUCATION.
AERONAUTICAL ENGINEERING
(SELECTED ARTICLES)

FOREIGN TECHNOLOGY DIVISION

AIR FORCE SYSTEMS COMMAND

WRIGHT-PATTERSON AIR FORCE BASE

OHIO

UNEDITED ROUGH DRAFT TRANSLATION

NEWS OF SCHOOLS OF HIGHER EDUCATION. AERONAUTICAL ENGINEERING (SELECTED ARTICLES)

English Pages: 41

SOURCE: Russian Perodical, Izvestiya Vysshikh Uchebnykh Zavedeniy. Aviatsionnaya Tekhnika, Nr 2, 1962, pp 65-71, 113-133, 138-151

S/147-62-0-2

THIS TRANSLATION IS A RENDITION OF THE ORIGINAL FOREIGN TEXT WITHOUT ANY ANALYTICAL OR EDITORIAL COMMENT. STATEMENTS OR THEORIES ADVOCATED OR IMPLIED ARE THOSE OF THE SOURCE AND DO NOT NECESSARILY REFLECT THE POSITION OR OPINION OF THE FOREIGN TECHNOLOGY DIVISION.	PREPARED BY: TRANSLATION SERVICES BRANCH FOREIGN TECHNOLOGY DIVISION WP-AFB, OHIO.

TABLE OF CONTENTS

STABILITY OF A CIRCULAR CYLINDRICAL ENVELOPE IN A NON-UNIFORM TEMPERATURE FIELD

V. V. Kabonov

The present article is devoted to the investigation of the linear problem of the local stability of a circular cylindrical envelope in the median surface of which act the longitudinal forces

$$T_1 = -T \cdot f(\varphi), \qquad (1)$$

where T is a parameter; $f(\varphi)$, an arbitrary even function of coordinate φ (Fig. 1). The forces (1) usually arise in long envelopes with non-uniform heating. The questions as to the effect of the non-uniformity of distribution of forces on the critical value of the peak force have not at present been sufficiently thoroughly elucidated. Only in the simplest case of a non-uniform field of forces — bending by torque — has it been established that for thin-walled envelopes the critical value of the peak force according to the linear theory is not substantially different from the critical force in axisymmetrical compression*. An attempt to investigate the problem in its general form has been made by Abir and Nardo [3]. The authors, however, as

---

* These results were obtained by Yu. G. Odinokov (Trudy KAI, 1940) and A. V. Karmishin, and also by Ye. D. Pletnikova (Trudy MAP, No. 677, 1949).

will be shown, were limited by investigating one essentially trivial case and did not solve the task set.

Let us note the stability equations from Vol'mir [2]:

$$D\nabla^2\nabla^2 W - \frac{1}{R}\cdot\frac{\partial^2 F}{\partial x^2} = T_1\cdot\frac{\partial^2 W}{\partial x^2},$$
$$R\cdot\nabla^2\nabla^2 F = -Eh\cdot\frac{\partial^2 W}{\partial x^2}. \tag{2}$$

We look for functions of W and F in the form of series:

$$W = \cos q\frac{x}{R}\cdot\sum_{n=0}^{\infty} C_n\cos n\varphi,$$
$$F = \cos q\frac{x}{R}\cdot\sum_{n=0}^{\infty} B_n\cdot\cos n\varphi, \tag{3}$$

where

$$q = \pi R/l, \tag{4}$$

and l is the length of the half-wave in a longitudinal direction. Substituting Expression (3) in the system of equations (2) and excluding B_n we find

$$\sum_{n=0}^{\infty} C_n\left[\frac{D}{R^2}\cdot\frac{(n^2+q^2)^2}{q^2} + Eh\frac{q^2}{(n^2+q^2)^2}\right]\cos n\varphi = -T_1\sum_{n=0}^{\infty} C_n\cos n\varphi. \tag{5}$$

Expanding the right side of this equality into a series and equalizing the coefficients with cos nφ we obtain an infinite homogeneous system of equations for determining the coefficients of C_n:

$$(1+\delta_{n,0})\cdot\pi a_n T_c\cdot C_n + \sum_{k=0}^{\infty} C_k\cdot\int_0^{\pi} T_1\cdot[\cos(k+n)\varphi + \cos(k-n)\varphi]\,d\varphi, \tag{6}$$
$$(n = 0,\ 1,\ 2\ldots),$$

where

$$a_n = \frac{h}{R}\cdot\frac{1}{\sqrt{48(1-\nu^2)}}\cdot\left(q_1^2 + 12\frac{R^2}{h^2}\cdot\frac{1-\nu^2}{q_1^2}\right),$$
$$q_1 = (q^2+n^2)/q,\quad T_c = Eh^2/R\sqrt{3(1-\nu^2)}, \tag{7}$$

and $\delta_{n,o}$ is Kronecker's symbol. For practical calculations it is more convenient to write System (6) in matrix form:

$$(\lambda E - A)\cdot C = 0, \tag{8}$$

where

$$E=\{1\},\quad A=\{\beta_{nk}/a_n\},\quad C=\{C_n\},$$

$$\lambda=\pi T_c/T,\quad \beta_{nk}=\int_0^{\pi} f(\varphi)\left|\cos(n+k)\varphi+\cos(n-k)\varphi\right|d\varphi/(1+\delta_{n,0}). \tag{9}$$

Thus, the problem of determining the critical force is reduced to finding the largest eigen-number λ of matrix A; characteristic vector C of matrix A determines the deflections by itself. Finding the largest eigen-number is conveniently done by the iterative method. To do this, the infinite matrix must be replaced by a finite one, of an order sufficient to guarantee the necessary accuracy. In calculating the length of the wave in a longitudinal direction we should carry out the minimalization in accordance with the parameter of wave formation q. Let us examine several particular cases.

1. $T = N$, $f(\varphi) = 1$ (uniform axial compression). From System (6) for this case we obtain the known formula (cp. Timoshenko [1]):

$$N = T_c \tag{10}$$

2. $T = M/R^2$, $F(\varphi) = \cos\varphi$ (bending by torque). From System (8) we may in the given case also obtain a known result:

$$M=\pi R^2\cdot T_c. \tag{11}$$

3. $T=Ek\alpha T^\circ,\quad f(\varphi)=t-t_0-t_1\cdot\cos\varphi,$ (12)

where

$$t_0=\frac{1}{\pi}\int_0^{\pi} t\,d\varphi,\quad t_1=\frac{2}{\pi}\int_0^{\pi} t\cdot\cos\varphi\,d\varphi. \tag{13}$$

$t = t(\varphi)$ is the even function; and α, the coefficient of linear expansion of the envelope material. This case corresponds to the temperature stresses in a long envelope having a temperature of $T^\circ \cdot t(\varphi)$.

From Expression (9) for the parameter of critical temperature we obtain the formula

$$T^\circ=k_2\cdot T_c^\circ, \tag{14}$$

where

$$k_2=1/\lambda,\quad T_c^\circ=\pi k/\alpha R\cdot\sqrt{3(1-\nu^2)}. \tag{15}$$

In accordance with (1), (12), and (14) we have the value of the critical force

$$T_1 = -k_1 \cdot \pi \cdot (t - t_0 - t_1 \cos\varphi) \cdot T_c. \qquad (16)$$

At some value of $\varphi = \varphi_0$ this force will be largest:

$$T_{1\max} = -k_2 \pi (t - t_0 - t_1 \cdot \cos\varphi_0) \cdot T_c. \qquad (17)$$

As an example, let us examine the practically important case of the stability of an envelope partially filled with a fluid at a temperature of zero situated in a medium with temperature T^0 (Fig. 1).

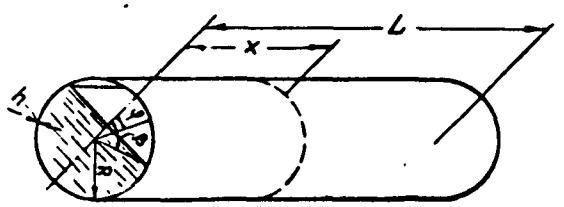

Fig. 1

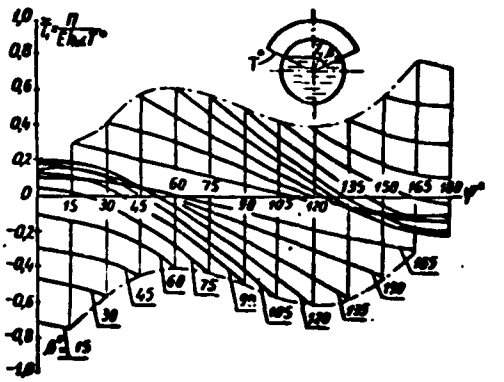

Fig. 2.

In the first approximation let us take

$$t(\varphi) = \delta(\varphi) = \begin{cases} 1 \text{ when } & 0 \leq |\varphi| \leq \beta_{-0} \\ 0 \text{ when } & \beta_{+0} \leq |\varphi| \leq \pi. \end{cases} \qquad (18)$$

The longitudinal force T_1 in accordance with relationships (1), (12), and (13) is determined by the formula

$$T_1 = -Eh\alpha T^0 \cdot [\delta(\varphi) - (1/\pi)(3 + 2\sin\beta \cdot \cos\varphi)]. \qquad (19)$$

The values of the relative forces $\overline{T}_1 = T_1/Eh\alpha T^0$ are shown in Fig. 2. For the coefficients β_{nk} and the critical forces T_1 we obtain the following expressions:

$$\beta_{0k} = \frac{\sin k\beta}{k} \cdot \delta_{k,p}, \quad \beta_{nk} = \frac{\sin(n+k)\beta}{n+k} \cdot \delta_{n+k,p} + \frac{\sin(n-k)\beta}{n-k} \cdot \delta_{|n-k|,p} \qquad (20)$$

$$(p > 2),$$

$$T_1 = -k_2 \cdot [\pi \cdot \delta(\varphi) - \beta - 2 \cdot \sin\beta \cdot \cos\varphi] \cdot T_c. \qquad (21)$$

We take the largest value of force T_1 when $\varphi = \beta$:

$$T_{1\max} = -k_2[\pi \cdot \delta(\varphi) - \beta - \sin 2\beta] \cdot T_c. \qquad (22)$$

In this, $\delta(\varphi) = 1$ corresponds to the positive values of T° (heating); and to the negative (cooling), $\delta(\varphi) = 0$. In Fig. 3 for $\beta = 15^\circ$ and $h/R = 10^{-2}$ to 10^{-3} the values of the smallest magnitudes of k_2 and of those of q^2 corresponding to them are entered as solid lines. The values of k_2 were calculated for a matrix of the fiftieth order on a "Ural" machine. As the calculations showed, a similar pattern occurs also for other values of β. In Fig. 4 curves have been constructed for $\beta = 15^\circ$ and 120° reflecting the change in deflections. It is evident from these curves that convexity occurs primarily in compressed zones.

From Fig. 3 it is evident that oscillation occurs along the short longitudinal waves so that q^2 is a large number. Taking $q^2 \gg n^2$ we may consider that α_n does not depend on n,

$$q \backsimeq q_1, \qquad (23)$$

and the critical temperature, in accordance with relationships (8), (14), and (15), are proportional to α_n. From the condition of minimum α_n we will determine

$$q_1 = (R/h) \cdot \sqrt{12(1-\nu^2)}. \qquad (24)$$

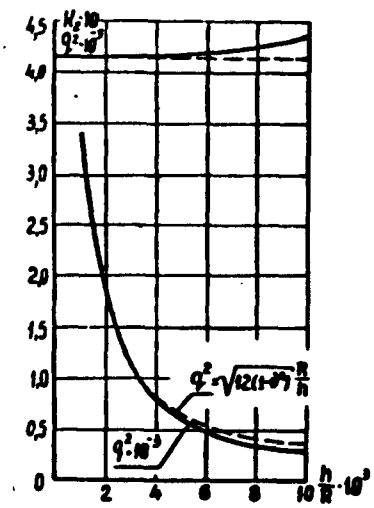

Fig. 3.

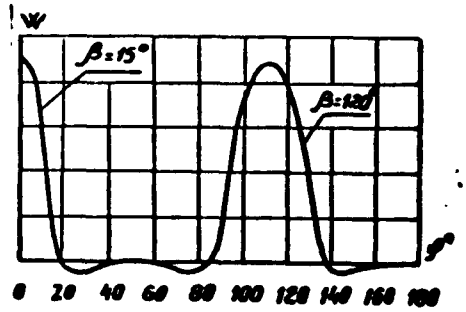

Fig. 4.

In doing this, $\alpha_n = 1$, k_2 does not depend on h/R, and consequently the critical temperature is proportional to h/R. We will show that in this case the maximum value of the critical force equals the value of the critical force in uniform compression. Let us examine the stability of an envelope in the mean surface of which act the forces

$$T_1 = -A_p \cdot \cos p\varphi, \ (p > 1). \tag{25}$$

Substituting expression (25) in equation system (6) we obtain

$$\lambda_p \cdot \alpha_0 \cdot C_0 = C_p, \tag{26}$$

$$\lambda_p \cdot \alpha_n \cdot C_n = C_{n+p} + C_{n-p}. \tag{27}$$

Here

$$\lambda_p = 2T_c/A_p. \tag{28}$$

We will examine Eq. (27) as an equation of finite differences. Its solution when $\alpha_n = 1$ has the form

$$C_n = B_1 \cdot P_1^{n/p} + B_2 \cdot P_2^{n/p},$$

where

$$P_{1,2} = (1/2) \cdot (\lambda_p \pm \sqrt{\lambda_p^2 - 4}).$$

Satisfying Eq. (26) and considering that at sufficiently large $n = k$ the coefficients of C_n approach zero, we will derive a system for determining the constants B_1 and B_2:

$$B_1 P_1^{k/p} + B_2 \cdot P_2^{k/p} = 0,$$

$$B_1 \cdot P_2 + B_2 \cdot P_1 = 0.$$

Setting the determinant of this system equal to zero we find

$$\lambda_p = 2, \text{ i.e. } A_p = T_c.$$

Consequently when $q^2 >> n^2$ is assumed, the non-uniformity of the force distribution along the section does not influence the critical value of the maximum force. In one work [3] this essentially trivial case was investigated, and the authors derived the value $A_p > T_c$.

Assuming $q^2 >> n^2$ we should consider

$$T_{1\max} = -T_c. \tag{29}$$

For the coefficient k_2 we have from Formula (17) the expression:

$$k_2 = 1/\pi(t - t_0 - t_1 \cdot \cos\varphi_0). \tag{30}$$

For the envelope examined in the example

$$k_2 = 1/[\pi \cdot \delta(\varphi) - \beta - \sin 2\beta]. \tag{31}$$

The values of k_2 for the positive values of T^0 are entered in Fig. 3 as a dotted line, as well as the values of q^2 corresponding to them according to Formula (23). As is evident from Fig. 3 the values of k_2 calculated in the assumption that $q^2 >> n^2$ are close to the true ones. There is a small deviation in the range of the larger values of h/R. Figure 5 shows the values of k_2 calculated from Formula (31). In this, the positive values of k_2 correspond to heating the envelope; the negative, to cooling.

From Fig. 5 it is clear that the lowest critical temperature corresponds to small angles of β. The values of k_2 corresponding to it may be obtained in the form of a formula not assuming $q^2 >> n^2$. We mentally separate the compressed panel from the envelope with the generatrices $\varphi = \pm\beta$. On the whole we assume for the envelope that oscillation occurs only in the compressed zone. Consequently,

$$w = 0 \text{ when } \varphi = \pm\beta. \tag{32}$$

We will present the deflections $\underline{w}$ which satisfy this condition in the following form:

$$w = C \cdot \cos q\frac{x}{R} \cdot \cos b_n\varphi, \tag{33}$$

where

$$b_n = \pi/2\beta, \quad q = \pi R/l. \tag{34}$$

From the second equation of system (2) we have

$$F = (EhCR/\beta_n^2)\cos q\frac{x}{R} \cdot \cos b_n \cdot \varphi, \tag{35}$$

where

$$\beta_n = (b_n^2 + q^2)/q = (\pi/2\beta)(b/l + l/b), \quad b = 2R\beta. \tag{36}$$

Substituting expressions (33) and (35) in the first equation of (2) and applying the Galerkin method we find

$$T^{\circ} = k_{21} \cdot (\pi/a)[(D \cdot \beta_n^2 / EhR^2) + 1/\beta_n^2], \tag{37}$$

where

$$k_{21} = 1/[\pi - \beta - [2\pi^2/(\pi^2 - \beta^2)] \cdot \sin^2\beta]. \tag{38}$$

From the condition of minimum T° let us determine

$$\beta_n^2 = (R/h) \cdot \sqrt{12(1-\nu^2)}. \tag{39}$$

Substituting this value in Formula (37) we get

$$T_2^{\circ} = k_{21} \cdot T_c^{\circ}. \tag{40}$$

The values of k_{21} in the small angle range of β ($\beta \leq 30^{\circ}$) are practically no different from the values of k_2.

Let us determine the lower limit for applying Formula (40). When β is a small angle the value of β_n is large. In expression (37) the first term is basic, consequently, minimum β_n will correspond to minimum T°. A minimum value will be assumed by β_n

$$\beta_{n\,min} = \pi/\beta. \tag{41}$$

when 1 = b. From the condition $\beta_n \geq \pi/\beta$ we get

$$\beta > \pi \sqrt{h/R} / \sqrt[4]{12(1-\nu^2)}. \tag{42}$$

At smaller values of β we should substitute β_n in expression (37) in accordance with Formula (41). Then

$$T^{\circ} = k_{22} \cdot T_c^{\circ}, \tag{43}$$

where

$$k_{22} = k_{21}\{[(h/R)(\pi^2/\beta^2)/\sqrt{48(1-\nu^2)}] + (\beta^2/\pi^2) \cdot (R/h)\}. \tag{44}$$

The qualitative change in the coefficient k_{22} in Fig. 5 is shown by the dotted line. When β tends toward zero we have

$$T^{\circ} = 4\pi^2 D/Eha^2. \tag{45}$$

In this case the panel bulges like a long flat plate compressed by a uniform force

$$T_1 = Eh\alpha T^{\circ}.$$

To resume what has been stated – we may note that within the limits of the linear theory of stability of thin-walled envelopes the non-uniformity in the distribution of forces in a cross-section of the envelope examined as an example has practically no effect on the critical value of the largest compressive force. Bulging of the envelope along short longitudinal waves occurs when the largest compressive force has reached the value of the critical force in uniform compression. We may consider the critical temperature to be proportional to h/R. Small deviations from that are observed in the range of large values of h/R. Under real conditions the temperature jump (18) is not realized in practice. Temperature stresses in the cross-section of the envelope will distribute themselves more uniformly than in the envelope examined. Consequently the effect of the non-uniformity in the distribution of stresses will be even less.

REFERENCES

1. S. P. Timoshenko. The Stability of Elastic Systems. OGIZ, Gostekhizdat, 1946.

2. A. S. Vol'mir. Flexible Plates and Envelopes. Gostekhizdat, 1956.

3. D. Abir and S. Nardo. Journal of the Aerospace Sciences, Vol. 26, No. 12, pp. 803-808, 1959.

A METHOD OF PROJECTING AND THE RESULTS OF INVESTIGATING A VANELESS DEFLECTOR FOR RADIAL-AXIAL TURBINES

A. V. Gubarev, et al.

At present centripetal turbines are made with vane deflectors. The elaboration of theoretical methods of calculation as well as experimental research have enabled us to attain a very high efficiency in directional screens of the radial type. In projecting turbines, however, great difficulties arise in organizing the stream on entry into the deflector, since in order to secure high efficiency of the screen it is necessary that the stream's angle of entry into it be close to the calculated one, in the majority of cases equalling 90°. As a result the dimensions of the supply nozzle (contraction) and consequently the weight of the unit sharply increases. The complexity of its manufacture may also be considered among the drawbacks of the vane deflector.

The vaneless deflector (Fig. 1) is simpler in structure and smaller in dimensions and weight. In order to understand the idea of a vaneless deflector it is sufficient to note the fact that in the

radial slot of a centripetal turbine the gas flow is subject to the law of vortical flow — the velocity of the gas increases toward the center. In this, with an increase in the radial slot the effect of the losses in a vane deflector on the efficiency of the turbine decreases. Consequently deflector screen efficiency may worsen somewhat without decreasing the efficiency of the unit as a whole, i.e., without decreasing the turbine efficiency we may increase the chord or relative travel of the grid compared to the optimum and decrease the number of vanes on the circumference. In addition, if the stream is up the radial slot behind the vane deflector the elevation of the grid is increased, and without lowering the efficiency of the deflector in comparison to the initial it proves to be possible to curtail substantially the number of vanes in the circumferential grid. In the limiting transition the conclusion suggests itself that it is possible to make a vaneless deflector. To do this the necessary circumferential stream velocity C_u on entering the wheel is secured from the tangential gas supply to helix with a definite velocity C_0; and the radial component of velocity C_a and consequently the given exit angle of the stream from the deflector are secured by the geometrical relationships of the helix and the circumferential accelerating region.

Calculation Methods and Choice of Basic Geometrical Relations

The flow of the gas in the helix of a vaneless deflector has a spatial nature. Therefore the elaboration of accurate methods of calculating it encounters great difficulties. The calculation is simplified if we introduce the following assumptions:

1) the gas is ideal ($\mu = 0$),

2) the distribution of flow parameters in the exit section of the

deflector is uniform*,

3) the parameters of the stream on exiting the supply nozzle and in every section of the helix are constant.

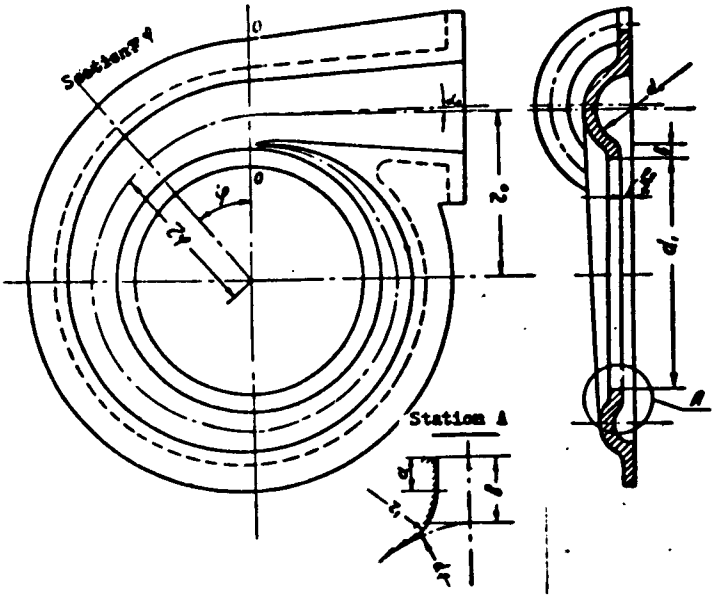

Fig. 1. Vaneless deflector

Taking these assumptions into consideration let us write the discontinuity equation for section F_0 on entering the helix and for the section on leaving the deflector in the following form:

$$\rho_0 C_0 F_0 = \rho_1 C_1 \pi d_1 l_1 \sin \alpha_1. \qquad (1)$$

Here the subscript 0 refers to parameters on entering the helix.

For the same sections we will write the equation resulting from the law of conservation of circulation in a potential vortex:

* This assumption in the case of solving the delicate problem of outlining the helix is the limiting condition.

$$C_0 r_0 \cos\alpha_0 = C_1 \frac{d_1}{2} \cos\alpha_1. \qquad (2)$$

Let us transform these equations to the form

$$q_0 F_0 = q_1 \pi d_1 l_1 \sin\alpha_1, \qquad (1')$$

$$\lambda_0 r_0 \cos\alpha_0 = \lambda_1 \frac{d_1}{2} \cos\alpha_1. \qquad (2')$$

In Eq. (2) we may with sufficiently great accuracy take $\alpha_0 = 0$*. Since

$$q = \left(\frac{k+1}{2}\right)^{\frac{1}{k-1}} \lambda \left(1 - \frac{k-1}{k+1}\lambda^2\right)^{\frac{1}{k-1}}, \qquad (3)$$

this system of equations may be solved if we additionally ascertain the relationship between the geometrical dimensions of the vaneless deflector.

From Fig. 1 it follows that

$$r_0 = \frac{d_1}{2} + b + \frac{d_0}{2}, \qquad (4)$$

where $b = \beta l_1$ is the width of the circumferential acceleration region.

For an incompressible fluid Eqs. (1) and (2) may be rewritten thus:

$$\frac{\pi d_0^2}{4} C_0 = \pi \bar{l}_1 C_1 \sin\alpha_1, \qquad (5)$$

$$C_0 \bar{r}_0 = C_1 \frac{\cos\alpha_1}{2}. \qquad (6)$$

Here the superposed line designates the dimensionless value $\bar{n} = n/d_1$.

From Eqs. (5) and (6) we may derive

---

* Angle α_0 must be taken into consideration in projecting the helix.

$$\bar{r}_0 = \frac{\cos \alpha_1}{2\gamma}, \tag{7}$$

$$\bar{d}_0 = 2\sqrt{\frac{\bar{l}_1}{\gamma}\sin \alpha_1}, \tag{8}$$

where $\gamma = C_0/C_1$.

Consequently the dimensions of the helix ($2\bar{r}_0 + \bar{d}_0$) essentially depend on parameter γ. Indeed, when γ decreases, $\bar{r}_0$ increases along the hyperbola (Fig. 2). It is necessary to mention that parameter γ also determines the expediency of using a vane deflector or vaneless deflector, since when $\gamma < 0.5$ the effect of the collector on the work of the vane deflector can practically be ignored.

We must solve the system of Eqs. (4), (7), and (8) to determine parameter γ. After the pertinent transformations we get:

$$\gamma = \frac{K_1 \pm \sqrt{K_1^2 - K_2^2 \cos^2 \alpha_1}}{K_2^2}, \tag{9}$$

where

$$K_1 = \cos \alpha_1 + 2\bar{l}_1(\beta \cos \alpha_1 + \sin \alpha_1),$$
$$K_2 = 1 + 2\beta\bar{l}_1.$$

In expression (9) the + sign corresponds to the flow of gas from the center to the periphery. This case does not interest us.

The calculated curves of the relationship of γ to $\bar{l}_1 = l_1/d_1$ for different stream exit angles α_1 from the deflector and several values of β are shown in Fig. 3 Analysis of them shows that the gain in the dimensions of the unit may be derived from a vaneless deflector at small values of l_1, α_1, and β. It should be noted that the value of β within known limits may be arbitrarily chosen. This problem, and the very expansion of the range of advisable application of vaneless deflectors, may be solved if we use a helix of elliptical or

rectangular cross-section or increase the number of supplying nozzles.

Using the graphs in Figs. 2, 3, and 4 it is easy to choose the basic geometrical parameters of the vaneless deflector in accordance with the prescribed characteristics of the stream on entering the working wheel. We actually know d_1, $l_1 = \bar{l}_1/d_1$, and α_1 from the thermal calculation of the turbine. Let us set as a goal the value of $\beta = b/l$. (We may recommend a value of β within the limits 0.2-0.6.) After this, we find the value of $\gamma = C_0/C_1$ from the corresponding graph (Fig. 3) and from Figs. 2 and 4 respectively we find

$$\bar{r}_0 \text{ and } \bar{d}_0.$$

The opposite problem, i.e., determining the gas dynamic characteristics from the given geometrical parameters of the vaneless deflector, may be thus resolved. Let us divide Eq. (5) by (6) termwise and after transformation we get

$$\tan \alpha_1 = \frac{\bar{a}_0^2}{8\bar{l}_1\bar{r}_0}.$$

Then from Figs. 2 and 4 we find $\gamma = C_0/C_1$ etc.

A detailed calculation of the deflector (profiling the helix) may be conducted as follows. Since we must secure uniform distribution of stream parameters in the exit section, the gas flow rate in a given section φ must be (Fig. 1)

$$G_\varphi = G_0 \frac{2\pi - \varphi}{2\pi},$$

where φ is the angle in radians.

Then Eqs. (4), (5), and (6) take the form

$$\frac{\pi \bar{a}_\varphi^2}{4} C_\varphi = \pi C_1 \bar{l}_1 \frac{2\pi - \varphi}{2\pi} \sin \alpha_1,$$

$$C_\varphi \bar{r}_\varphi \cos \bar{\alpha}_\varphi = C_1 \frac{\cos \alpha_1}{2},$$

$$\bar{r}_\varphi = \frac{1}{2} + \bar{e} + \frac{\bar{a}_\varphi}{2}.$$

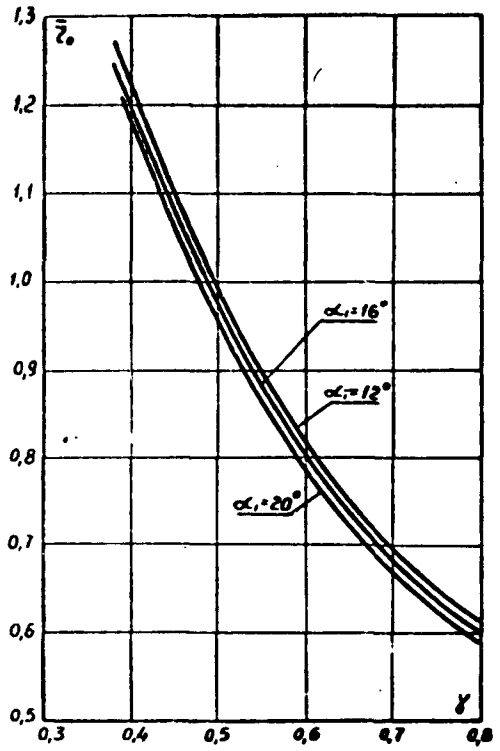

Fig. 2. Change of radius $\bar{r}_0$ in relationship to the coefficient of acceleration $\gamma = C_0/C_1$ of the calculated angle of exit of stream α_1.

Here as in Eq. (6) we may take $\cos \alpha_\varphi = 1.0$.*

Solving the quoted system of equations we obtain the following calculation formulas:

$$\bar{d}_\varphi = \frac{2\pi-\varphi}{2\pi}\,\frac{\frac{\bar{d}_0^2}{2}+\sqrt{\frac{\bar{d}_0^4}{4}+\frac{8\pi\bar{r}_0}{2\pi-\varphi}\bar{d}_0^2\left(\bar{r}_0-\frac{\bar{d}_0}{2}\right)}}{2\bar{r}_0}, \quad (10)$$

$$\bar{r}_\varphi = \bar{r}_0 - \frac{\bar{d}_0}{2} + \frac{\bar{d}_\varphi}{2}. \quad (11)$$

A consideration of the influence of compressibility on the gas dynamic characteristics is of especial interest for the vaneless deflector. Actually, as is easy to ascertain, the system of Eqs. (1), (2), and (3) for a compressible fluid is soluble only by the method of successive approximations. Therefore it is simpler in the beginning to calculate the vaneless deflector from the graphs listed in the work and then to introduce the appropriate correction for compressibility. This question is also of independent interest from the point of view of a variable regime of turbine work.

Let us designate the exit angle of the stream from the deflector in a flow of an incompressible fluid as α_1 (here and in the following

---

* In the present work no allowance is made for the change in α_φ along the helix. This drawback may be eliminated. But the complication in the methods connected with this may be justified only after conducting the corresponding experimental work.

the subscript 1 refers to an incompressible fluid).

From Eqs. (1), (2), (1'), and (2') may be derived the following equation:

$$\frac{\tan\alpha_1}{\tan\alpha_{i1}} = \frac{\rho_0}{\rho_1} = \left(\frac{1-\frac{k-1}{k+1}\lambda_0^2}{1-\frac{k-1}{k+1}\lambda_1^2}\right)^{\frac{1}{k-1}}. \qquad (12)$$

On the other hand we derive the following from Eqs. (2) and (2'):

$$\gamma = \frac{\lambda_0}{\lambda_1} = \gamma_a \frac{\cos\alpha_1}{\cos\alpha_{i1}}.$$

We may show that with large values of α_1 and when $\lambda_1 < 1$, γ is equal to γ_1. Equation (2) may then be written

$$\frac{\tan\alpha_1}{\tan\alpha_{i1}} = \left(\frac{1-\frac{k-1}{k+1}\gamma_a^2\lambda_1^2}{1-\frac{k-1}{k+1}\lambda_1^2}\right)^{\frac{1}{k-1}}, \qquad (13)$$

where γ_1 and α_{i1} are values known from the calculation of the incompressible fluid.

Figure 5 shows the calculated values of the dependence of tan α_1/tan α_{i1} on λ_1 and γ. Hence it follows that the greatest effect of λ_1 on the exit angle of the stream α_1 is observed at small values of γ.

We should note that the proposed method of determining the stream exit angle for a compressible fluid may also be used for vane deflectors. To do this it is enough to substitute the value of γ_1 in (13); and γ_1 is determined from the ratio of the radius of the circumference passing through the middle of the exit sections of the inter-vane channels to the diameter of the wheel, and to the stream exit angle for an incompressible fluid.

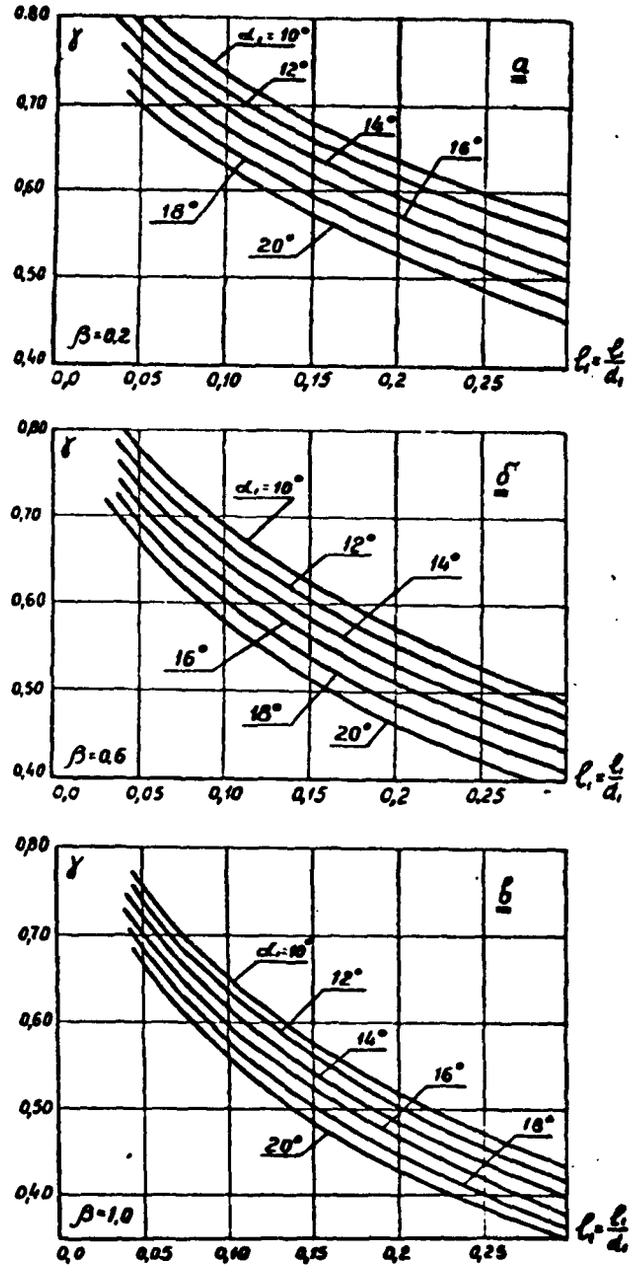

Fig. 3. Change in $\gamma = C_0/C_1$ in relationship to height of deflector and angle of exit of stream α_1.

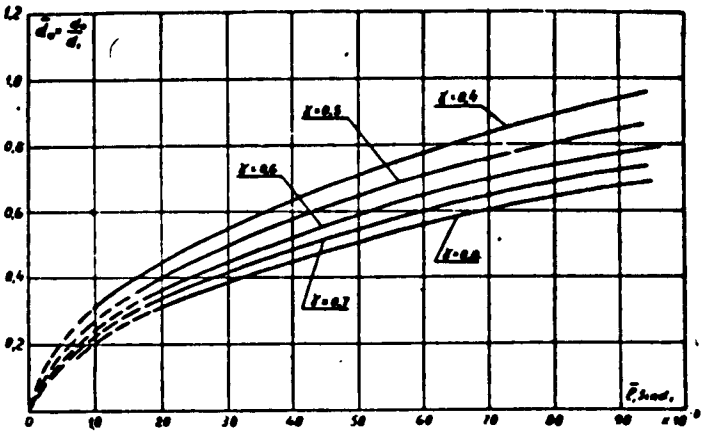

Fig. 4. Change in exit diameter of supply nozzle $d_o = d_o/d_1$ in relationship to $\gamma = C_o/C_1$ and to effective area of exit section of vaneless deflector $\bar{f}_1 \sin \alpha_1$.

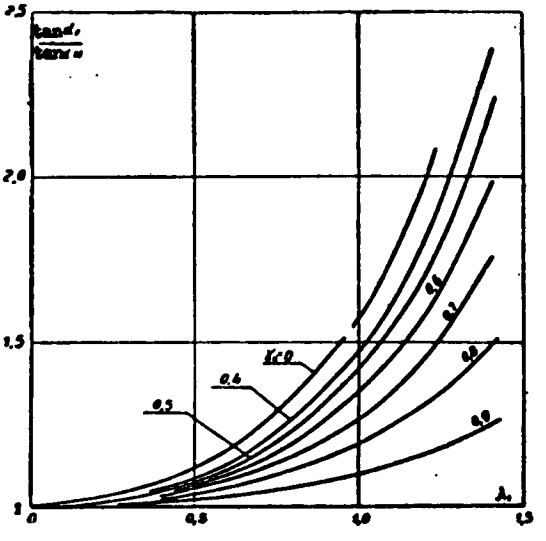

Fig. 5. Effect of compressibility on stream exit angle α_1 from vaneless deflector.

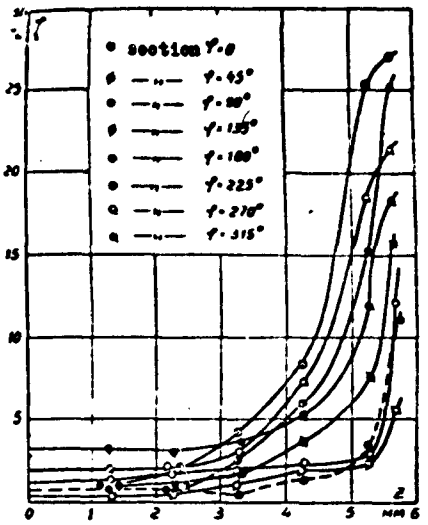

Fig. 6. Distribution of losses along exit section of vaneless deflection.

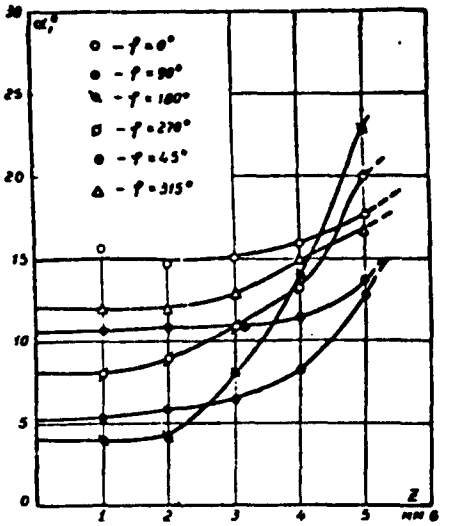

Fig. 7. Distribution of stream exit angles along exit section of vaneless deflector.

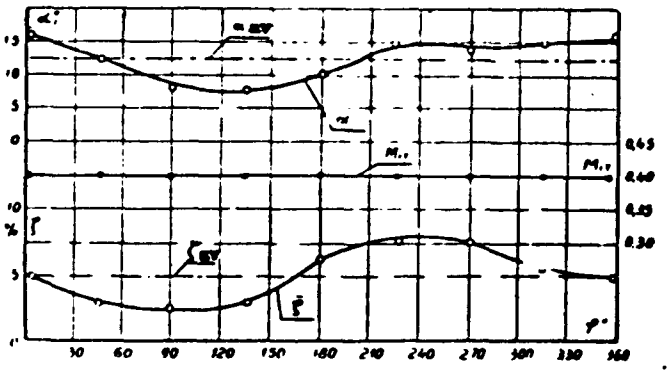

Fig. 8. Distribution of losses averaged on elevation and of stream exit angles along evolute of vaneless deflector.

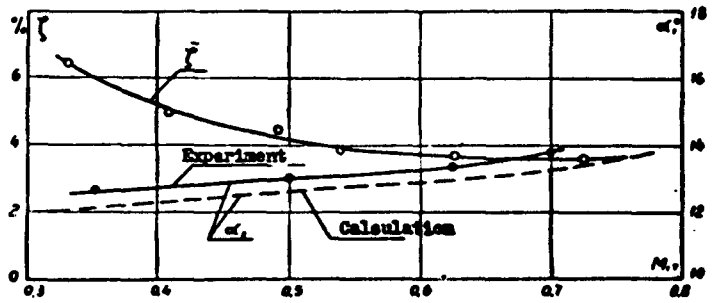

Fig. 9. Change in losses and stream exit angles for vaneless deflector as function of M number.

Results of Experimental Investigation

The investigated model of a vaneless deflector is characterized by the following parameters: $d_1 = 130$ mm, $l_1 = 12$ mm, and $\alpha_{1l} = 12^\circ$.

We determined experimentally the energy losses in 16 sections along the circumference (every 22.5°), the stream exit angles, and the static pressure in these sections. Measurements of pressure in the supply nozzle and on the center line along the helix were also made.

Figure 6 shows the curves of the distribution of losses along the elevation of the deflector. An examination of the curves shows that in the center sections the losses are small (0-1.5%), then sharply increase and in the region toward the end (z = 5-6 mm) reaches 20%. This is caused by frictional losses on the wall of the helix and of the circumferential acceleration region. When the M number is increased the distribution of losses on the elevation proves to be more uniform and the losses sharply decrease in the region toward the end.

Figure 7 shows the distribution of the stream exit angles on the elevation of the deflector in the different sections around the circumference. It is evident that the distribution of the stream exit angles is also very non-uniform along the exit section of the vaneless deflector. This is explained by the presence in the helix of greatly developed secondary flow (non-uniformity on the elevation) and by substantial deviations of the prepared model from the calculations (non-uniformity along the circumference). Measurements of the model showed that when $\varphi > 180^\circ$ the diameters of the helix sections differ from the calculations by 15-40%, and in connection with this there also occurred redistribution of the stream around the

circumference. The curves (Fig. 8) of the distribution of stream exit angles averaged on the elevation as a function of φ show the discrepancies agree sufficiently well with the permissible inaccuracy in the manufacture of the helix.

Figure 8 also shows the curves of losses averaged on the elevation in each section φ. Maximum losses are observed in sections φ = 220-270°, i.e., where the boundary layer in the helix attains great thickness. The field of velocities (static pressures) along the circumference of the vaneless deflector is uniform.

The losses (Fig. 9) averaged for the whole cross-section of the vaneless deflector are small (4-6%), noticeably decreasing with an increase in the M number. It is necessary to note that the efficiency of the vaneless deflector is the same as that of the vane deflector with a sufficiently greatly developed contraction at the entrance. Investigations of a vane deflector of the same dimensions showed that losses in it increased by 10-15%. Consequently the advantage of the vaneless deflector is obvious.

Figure 9 also lists the experimental and calculated curves of stream exit angle change. As is evident, the correspondence of the calculation and the experiment is sufficiently good.

Conclusions

1. The elementary methods of calculating the vaneless deflector which have been worked out enable us to define with sufficient accuracy the geometric parameters necessary for the designer and also to solve the converse problem and calculate the variable work regime.

2. The stream exit angle from the vaneless deflector depends on velocity λ_1 even at pre-critical temperatures.

3. The efficiency of the vaneless deflector and of the vane

deflector with a developed collector is practically the same. Consequently the vaneless apparatus permits us substantially to lower the weight and dimensions of the deflector of a radial-axial turbine without lowering its efficiency. In addition the technology of constructing the deflector is made easier.

4. The results obtained show the necessity of careful preparation of the helix, since, when its geometry deviates from that calculated, the field of velocities entering the turbine wheel is distorted.

5. The investigations carried out do not allow us sufficiently clearly to determine the limits of advisable use of the vaneless deflector. But the advisability of its use does not evoke any substantial objections.*

Further work must evidently be done toward improving the flow-through part of the helix and establishing the limits of use of the vaneless deflector. Investigations in the experimental turbine are also of great interest.

Steam and Gas Turbine Department Received November 17, 1961

---

* In Gas and Oil Power (January, 1961) it is reported that a firm has started manufacturing radial-axial turbines with vaneless deflectors. According to the advertisement the efficiency of this turbine is higher than one employing a vane deflector. It is noted that the use of vaneless deflectors permitted a lowering of the cost-price of the turbine and also a rise in the initial temperature to 870°.

CHARACTERISTIC THROTTLING FEATURES OF SINGLE-SHAFT BYPASS TURBOJET ENGINES IN DIFFERENT CONTROL PROGRAMS

A. L. Klyachkin and A. G. Smirnov

1. Introduction

In connection with the rapid development and introduction into operation of bypass turbojet engines it is of considerable interest to study the properties and peculiarities of the throttling characteristics of these engines. In the present article the throttling characteristics of a single-shaft bypass turbojet engine under various control programs are examined and an analysis is made comparing these characteristics with those of a straight turbojet engine. Research was conducted for stand conditions (H = 0 and M_0 - 0) and flight conditions (H = 5000 m and M_0 - 0.8). It makes it possible to determine the operating features of the engine in starting and cruising regimes, to discover possible functional limitations, and to find means of improving engine efficiency when choking the thrust.

Initial Data

As research subjects were chosen a "reference" turbojet engine

and a "derivative" bypass turbojet engine with a high-pressure compressor in the first stage (Fig. 1). In the calculated (nominal) regime ($H = 0$, $M_0 = 0$) the engines compared had the following parameter values for operation, efficiency, and loss factors:

$$T^*_{3(0)} = 1200^\circ, \text{ also } \pi^*_{sI(0)} = 15,$$
$$\eta^*_{t(0)} = 0{,}9, \quad \eta^*_{c(0)} = 0{,}838, \quad \sigma^*_{a} = 0{,}97, \quad \sigma^*_{ss} = 0{,}97,$$
$$\xi_{ss} = 0{,}97, \quad \varphi_{ja} = 0{,}97.$$

In the same regime the parameters of the bypass turbojet engine had the following values

$$\pi^*_{sII(0)} = 2.0 \text{ and } y_{(0)} = 2.0.$$

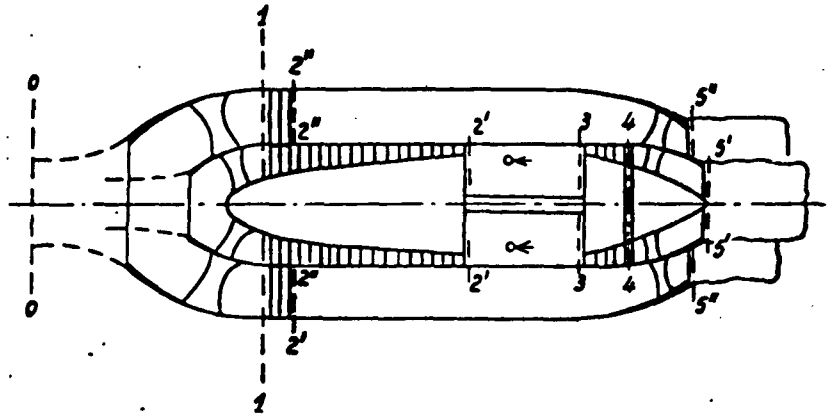

Fig. 1. Diagram of bypass of turbojet engine.

The selection of the degree of compression in the compressor of the second stage provided an approximately optimum distribution of energy between the stages. The values of the characteristic parameters of a cycle and of the individual properties of the bypass turbojet and of the straight turbojet in the regime calculated are listed in the table.

The characteristics of the compressors of the first and second are shown in Figs. 2 and 3.

Research Methods

The methods of calculating the characteristics of single-shaft bypass turbojets are worked out and described in Klyachkin [1]. Among the most important assumptions made in the course of the investigation are:

1) the presence of a critical pressure jump in the first nozzle unit of the turbine, i.e., $q(\lambda_{nu}) = 1$;

2) constant turbine efficiency, i.e., $\eta_t^* = \text{const}$;

3) constant loss factors σ_a^*, σ_{ss}^*, φ_{jn}, and ξ_{ss}.

Moreover, in all these calculations average and invariable values of the indices of the adiabatic curve in compression and expansion were assumed, i.e., $k_c = 1.4 = \text{const}$ and $k_e = 4/3 = \text{const}$.

TABLE

Values of Characteristic Cyclic Parameters and Individual Properties of Bypass Turbojet and Straight Turbojet Engine in Calculated Regime ($n = n_{nom}$, $H = 0$, $M_0 = 0$)

Parameter		π_k^*	π_t^*	τ_{jn}	T_2^*	T_3^*	T_4^*	R_{sp}	C_{sp}	Note
Straight turbojet		15	4.87	2,9	690	1200	851	67,1	0,786	
Bypass turbojet	Stage I	15	10,2	1.395	690	1200	723	36,1	—	$C_{sp\ bypass} = 0{,}499$
	Stage II	2	—	1,94	362	—	—	35,1	—	$R_{sp\ bypass} = 35{,}5$

Individual consumption of fuel was calculated with Vukalovich's tables of specific heat listed in Dmitriyev [2].

The characteristics of the bypass and straight turbojet engine were expressed as curves of relationships of absolute and also of relative parameters of the functioning and efficiency of the engine to its degree of thrust choking $R = R/R_{nom}$.

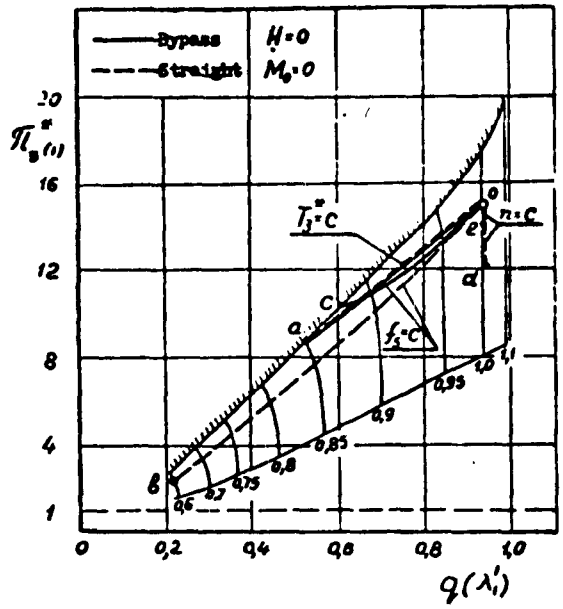

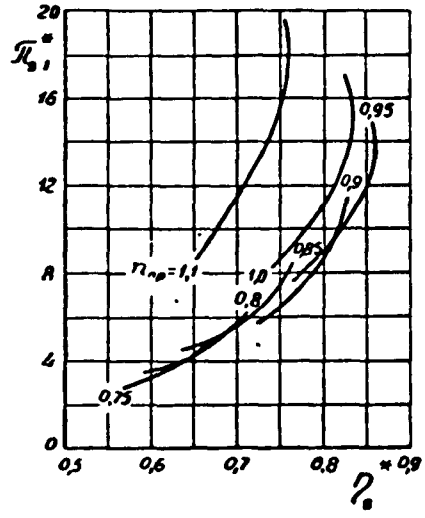

Figs. 2, 2a. Characteristics of first-stage compressor.

Engine Control Programs

The investigation of the throttling characteristics of a bypass and straight turbojet engine was conducted for three control programs:

1) invariable engine geometry ($f_5^I = c$ and $f_5^{II} = c$); 2) invariable number of revolutions ($n = c$ and $f_5^{II} = c$); 3) invariable temperature ($T_3^* = c$ and $f_5^{II} = c$).

In control programs (2) and (3) the invariable values of parameters n and T_3^* were maintained by the use of an adjustable nozzle in the first (basic) stage.

2. Effect of the Control Programs on the Course of Flow Lines in the Work Regime of Compressors of the First and Second Stage

The equation of the flow line of the work regimes of the compressor of the first stage of a bypass turbojet engine represents the solution of two equations:

flow rate

$$\tau_{\beta 1}^{\cdot} = \frac{f_1' q(\lambda_1')}{f_{вх} q(\lambda_{вх})} \sigma_{вх}^{\cdot} \sqrt{\frac{T_3^{\cdot}}{T_в^{\cdot}}} \qquad (1)$$

and steadiness of operation

$$\frac{c_p}{\lambda} T_3^{\cdot}\left(1 - \frac{1}{\pi_\beta^{\cdot \frac{n-1}{n}}}\right)\eta_\beta^{\cdot} = L_{в1} + \frac{\tau_{в11}^{\cdot}}{\tau_{в1}^{\cdot}} \sqrt{\frac{T_в^{\cdot}}{T_2^{\cdot II}}} \cdot \frac{f_5^{II} q(\lambda_5^{II})}{f_{вх} q(\lambda_{вх})} \cdot L_{в11}. \qquad (2)$$

In the control program $T_3^* = c$ (under the condition of $T_n^* = T_o = $ = const) the flow lines of the work regimes of the bypass and straight turbojet engine are completely congruent and are represented by the same o-a straight line. They are limited by "pumping."

In the control program $f_5 = c$ the flow lines of the work regimes are represented for straight turbojets by the curve o-b and for bypass turbojets by the curve o-c. The higher the degree of bypass, the more sloping the flow lines of the work regimes for the bypass turbojet and the larger the number of revolutions at which compressor "pumping" occurs.

Finally in the control program of n = c the flow lines of the work regimes of the bypass (o-e) and the straight (o-d) turbojet coincide. But even when the nozzle of the first stage of the bypass turbojet is slightly opened the pressure difference in this stage falls to 1 (point e)*, while the expansion capability of the jet nozzle of the straight turbojet is exhausted (point d) at a considerable greater opening of the nozzle and at correspondingly low values of π_{sI}^*.

The Second Stage Compressor

The equation for the flow lines of the work regimes of second stage the compressor of the bypass turbojet has the form found in Klyachkin [1]:

$$\pi_{s\,II}^{\cdot} = \left[\frac{f_1^{II} q(\lambda_1^{II})}{f_5^{II} q(\lambda_5^{II})\, \varepsilon_{comp}^{\cdot\,II}}\right]^{\frac{2n}{n+1}}, \qquad (3)$$

where n is the index of compression polytropy in the compressor.

In control programs (1) and (3) the work regime flow lines are

---

* That is, $p^*/p_n = 1$.

represented by the same parabolic curve o-f, and in program (2) the flow line of the work regimes has its origin at point 0.

3. Effect of the Control Programs on the Change in Parameters in the Function of Bypass and Straight Turbojet Engines in Choking ($M_0 = 0$, $H = 0$)

Let us examine the effect of the control programs on the change in the basic parameters in the functioning of bypass and straight turbojets when choked on the stand.

The change in y (Fig. 4)

In the control program $n = \text{const}$ and $f_5^{II} = \text{const}$, and also in the vertical characteristics of the first stage compressor the flow rate of air through each of the stages remains invariable. Consequently

$$y = G_{II}/G_I = \text{const}.$$

In the control program where $f_5^I = c$ the air flow rate through the second low pressure stage drops more gradually with the decrease in revolutions than it does through the first high-pressure stage; consequently, the degree of bypass of the engine increases as the choking so that we find $\bar{y} = 1.46$ when $\bar{R} = 0.64$ and $\bar{n} = 0.86$.

There is a similar relationship $\bar{y} = f(\bar{R})$ for the control program $T_3^* = \text{const}$.

The Change in π_t^* (Fig. 5)

When the jet nozzle in the first stage is opened (with $n = \text{const}$) the pressure differential in bypass and straight turbojets rapidly increases causing a drop in the temperature of the gas in front of the turbine.

When $f = c$ and the number of revolutions is decreased the pressure

differential in the straight turbojet stays constant in a wide range of thrust values (to $\bar{R} = 0.5$) until the pressure differential in the jet nozzle remains critical; on further decrease in revolutions the value of π_t^* is already falling. In a bypass turbojet for which $\pi^*_{jnI(0)} < 1.85$ the drop in π_t^* begins suddenly, as soon as choking of the engine begins.

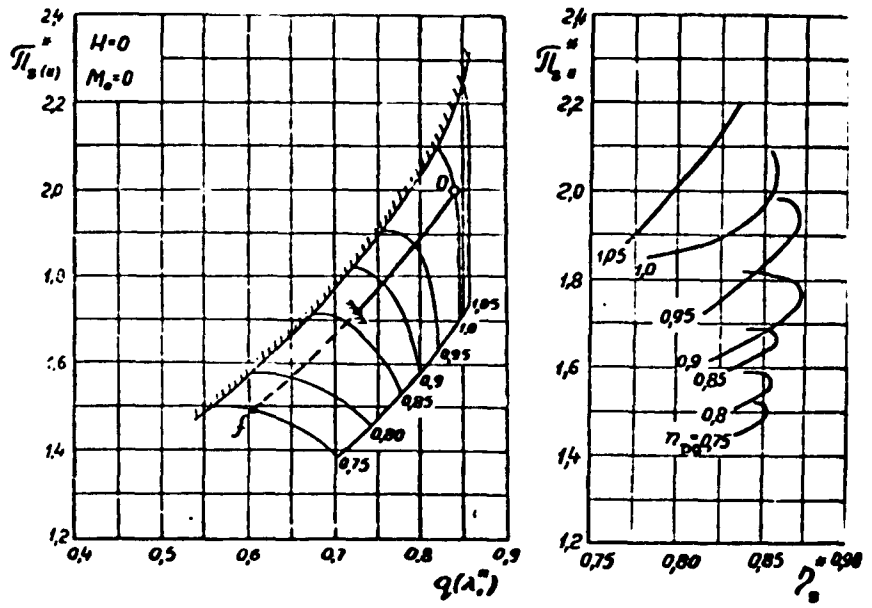

Figs. 3, 3a. Second stage compressor characteristics.

Finally, when $T_3^* = \underline{c}$ the decrease in π_t^* occurs more intensely, since maintenance of a constant gas temperature in front of the turbine is achieved because the jet nozzle of the first stage is throttled.

The Change in T_3^* (Fig. 6)

When the jet nozzle of the first stage is opened (control program $\underline{n} = \underline{c}$) the gas temperature in front of the engine turbine drops. The decrease in T_3^* proves to be less intense in the bypass turbojet, for which it reaches the value of sharp decrease in temperature

differential in the jet nozzle of the first stage and consequently of rapid drop in thrust.

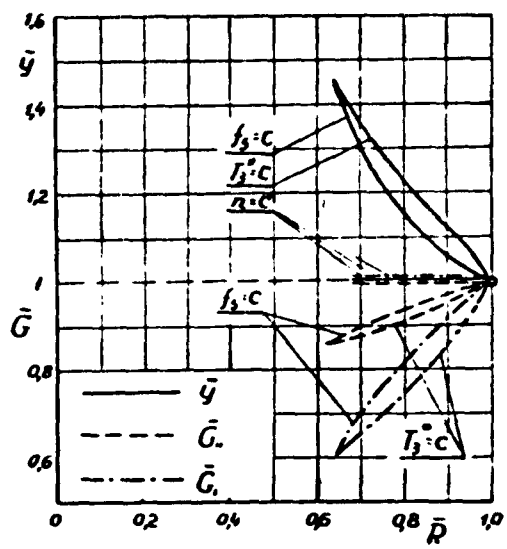

Fig. 4. Change in degree of bypass in throttling.

With the decrease in number of engine revolutions when f_5 = const the temperature of the gas in front of the turbine of the straight turbojet uninterruptedly falls in the range of thrust change (to $\bar{R} \approx$ $\approx$ 0.2). In the bypass turbojet the value of T_3^* at first decreases somewhat and then increases intensely as the engine is throttled. The latter circumstance is explained by the unfavorable change in the steadiness of the work at the turbocompressor of the engine: on one hand the compressor tightens as a result of the increase in the degree of bypass and on the other the turbine loosens because of the decrease of the pressure differential on it.

The Change in π_{sI}^* (Fig. 7)

Corresponding to the flow of the line of the work regimes on the first stage compressor characteristics the range of decrease in π_{sI} without the appearance of limitations on the work is greater in the straight turbojet than in the bypass turbojet (with the exception of program $T_3^* = \underline{c}$).

When $\underline{n} = \underline{c}$ and $\bar{R}$ = idem the degree of compression in the compressor of the first stage of the bypass turbojet is greater than in the straight turbojet; this is explained by the great thrust sensitivity of the bypass turbojet to the opening of the jet nozzle. When

$f_5 = \underline{c}$ and $\bar{R}$ = idem we have π^*_{sI} bypass < π^*_{sI} straight.

4. Effect of the Control Programs on the Change in the Individual Parameters of the Bypass and Straight Turbojet Engine When Throttled ($M_0 = 0$, $H = 0$)

The Change in Specific Thrust (Fig. 8)

The drop in the specific impulse of the straight turbojet engine on throttling takes place most intensely when $\underline{n} = \underline{c}$ (because of the simultaneous decrease in T^*_3, π^*_{sI}, and η^*_s) and somewhat more slowly when $f_c = \underline{c}$. In the case of $T^*_3 = \underline{c}$ when full thrust is decreased the specific thrust of the straight turbojet remains practically constant.

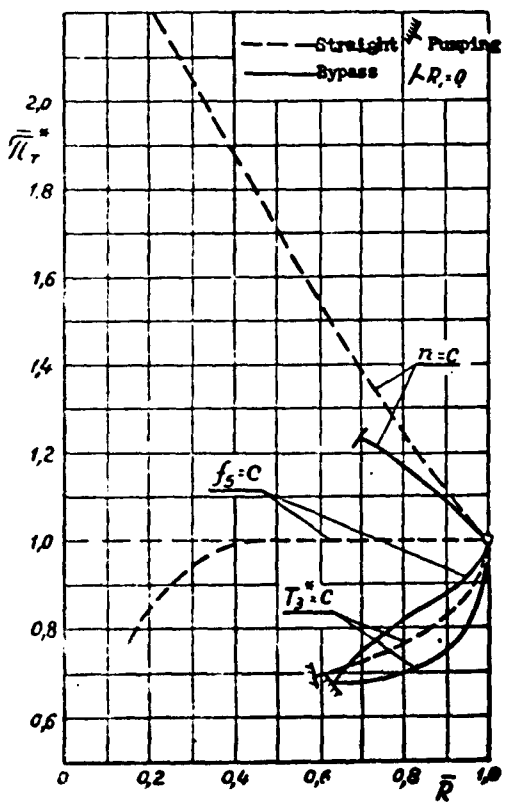

Fig. 5. Change in pressure differential in the turbine on throttling.

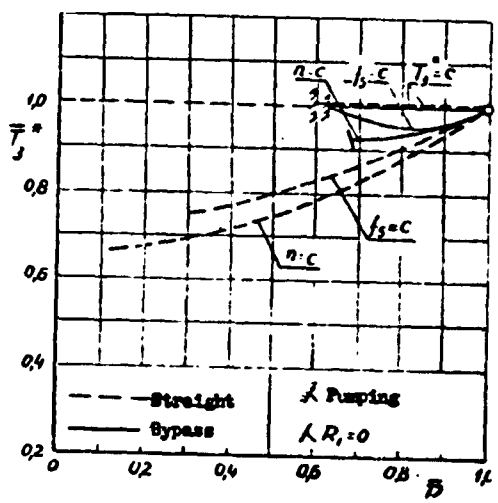

Fig. 6. Change in temperature of gases in front of turbine on throttling.

In the control programs of $\underline{n} = \underline{c}$ and $f_s = \underline{c}$ the patterns of the drop of specific thrust in the bypass turbojet and the straight turbojet coincide, but the limitations occurring in the bypass turbojet narrow the throttling range of the engine.

In the case of $T_3^* = \underline{c}$ and $\bar{R}$ = idem the relative specific thrust of the straight turbojet proves to be considerably less than in the straight turbojet. This is explained by the more rapid reduction of the specific thrusts in the stages of the derivative bypass turbojet in comparison with the specific thrust of the reference straight turbojet.

In the other control programs, however, the reduction in the individual thrust of the separate stages of the bypass turbojet mutually compensate each other (in comparison with the straight turbojet).

The Change in Relative Fuel Consumption (Fig. 9)

The change in relative fuel consumption

$$\bar{m}_{t(n)} \sim \overline{(T_3^* - T_2^*)}$$

when the bypass and straight turbojets are throttled is completely determined by the pattern of the temperature change:

$$\bar{T}_3^* = f(\bar{R}) \text{ and } \bar{T}_2^* = f(\bar{R}).$$

When $\bar{T}_3^* = \text{const}$ the curves of $\bar{m}_t = f(\bar{R})$ for the bypass and straight turbojets practically coincide (corresponding to the coincidence of the relation $\pi_{sI} = f(\bar{R})$.

The sharpest drop in $\bar{m}_t$ is observed in the control program $\underline{n} = \underline{c}$ in the straight turbojet and to a lesser degree in the bypass turbojet.

The Change in the Specific Consumption of Fuel ($M_0 = 0$, $H = 0$)

Figure 10 shows the change in the specific consumption of fuel when throttling the bypass and the straight turbojets in different control programs.

The curves of $f_5 = \underline{c}$ and $\underline{n} = \underline{c}$ for the straight turbojet have a clearly pronounced minimum of relative fuel consumption, the most advantageour being the control program of $\underline{n} = \underline{c}$, for which $\bar{C}_{sp(min)} = 0.84$ when $\bar{R} = 0.5$ to 0.6.

In the bypass turbojet the most rational control program is that of $f_5 = \underline{c}$. At a weakly pronounced cruising regime, however, ($\bar{R} = 0.9$) this program permits a very inconsiderable decrease in relative fuel consumption ($\bar{C}_{sp} = 0.975$). When throttling the bypass turbojet according to the programs of $T_3^* = \underline{c}$ and $\underline{n} = \underline{c}$, however, specific fuel consumption continuously increases.

The use of control programs $T_3^* = \underline{c}$ at cruising regimes in the bypass and straight turbojets proves to be irrational.

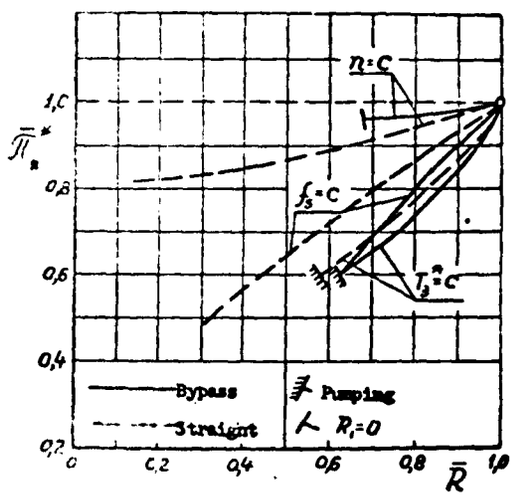

Fig. 7. Change in degree of compression in first stage compressor on throttling.

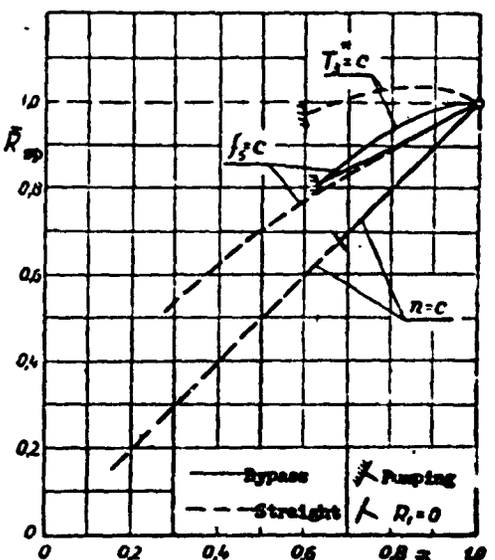

Fig. 8. Change in specific thrust in bypass turbojet stages on throttling.

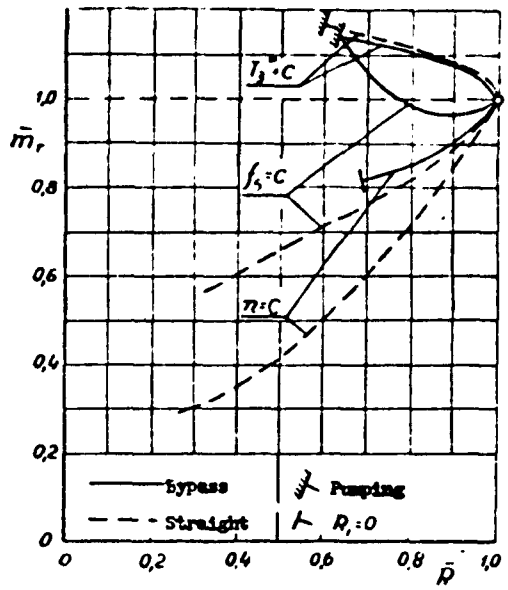

Fig. 9. Change in relative fuel consumption on throttling.

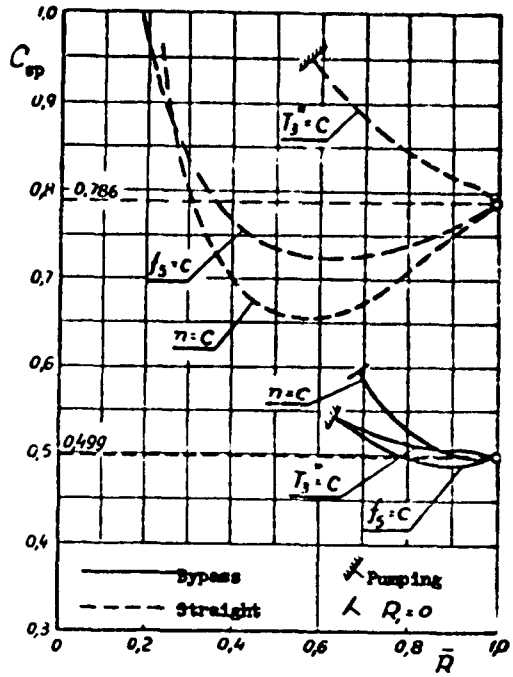

Fig. 10. Change in specific fuel consumption when throttling on stand.

The Effect of the Control Programs on the Redistribution of Thrust in the Bypass Turbojet Between the Stages on Throttling

When throttling the bypass turbojet in accordance with the three control programs examined, the thrust of the second stage rises comparatively (Fig. 11).

In the case of $\underline{n} = \underline{c}$ the thrust of the second stage preserves its numerical value but that of the first stage falls the most sharply.

The redistribution of the thrust between the stages when using the programs $f_5 = \underline{c}$ and $T_3^* = \underline{c}$ proves to be approximately the same.

The relative thrust increase of the second stage is explained by the redistribution of energy between the stages and is expressed by the degree of compression in the compressor proving to be considerably larger than the optimum during throttling.

5. Features of Throttling Characteristics of the Bypass Turbojet Engine in Flight* ($M_0 = 0.8$, $H = 5000$ m)

With an increase in the speed of flight there establishes itself under the effect of velocity pressure in the jet nozzle of the first stage of the bypass turbojet a critical temperature differential which is preserved even at a considerable degree of throttling (to $\bar{R} \approx 0.75$). Owing to this, the degree of gas expansion in the turbine of the bypass turbojet in flight ($M_0 > 0$, $H > 0$) turns out to be essentially greater, the temperature of the gas in front of the turbine is correspondingly lower than on the stand ($M_0 = 0$, $H = 0$). This means that the line of the work regimes of the bypass turbojet in flight takes a course more favorable for the characteristics of the compressor, the danger of appearance of pumping is eliminated, the characteristics of specific fuel consumption improve (economical work regime appears), and the range of operating regimes in which the bypass turbojet maintains its efficiency advantage over the straight turbojet becomes broader. Thus, in flight the throttling characteristics of a single-shaft bypass turbojet engine noticeably improve (Figs. 12 and 13).

---

* The throttling characteristics are of the greatest interest in analyzing the work of the engine on the stand ($M_0 = 0$, $H = 0$), but, since under high-speed conditions ($M_0 > 0$, $H > 0$) throttling of the engine's thrust also occurs (in flight cruising regime the thrust necessary to the airplane proves to be less than the maximum available engine thrust), use of the throttling characteristics allows us to select a control program of optimum efficiency.

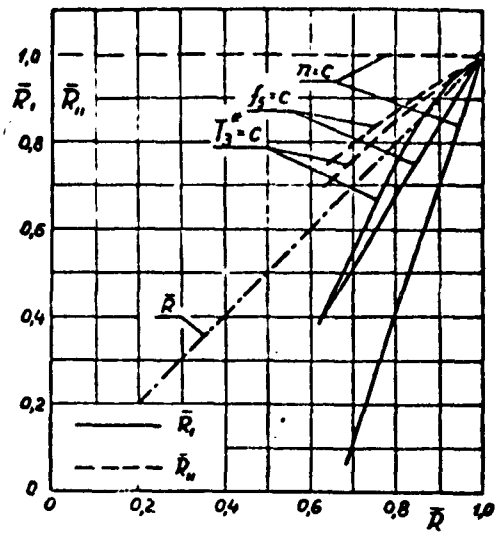

Fig. 11. Thrust redistribution between stages when throttling.

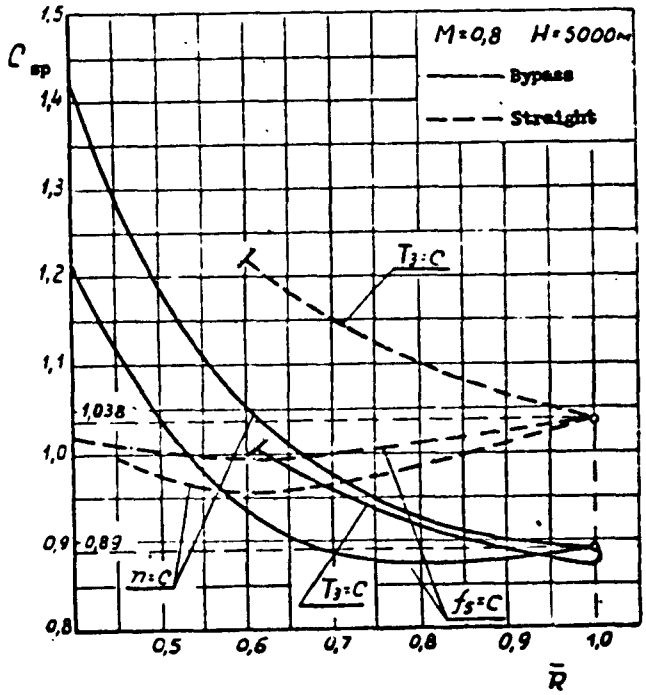

Fig. 12. Comparison of specific fuel consumption of bypass and straight turbojet in flight in different control programs.

6. Conclusions

1. At a high degree of bypass the characteristics of the single-shaft bypass turbojet engine permit an inconsiderable degree of thrust choking ($\bar{R}_{min}$ = 0.6 to 0.7) as a result of the limitations to the work of the engine which appear. Among these belong the phenomenon of pumping in the first stage compressor (control programs $f_5 = \underline{c}$ and $T_3^* = \underline{c}$), exhaustion of the first stage jet nozzle's power of expansion, and attainment of the limiting temperature of the gas T_3^*.

2. In the control programs $\underline{f} = \underline{c}$ and $\underline{n} = \underline{c}$ the throttling of the bypass turbojet is accompanied by continuous increase in its degree of bypass. This cause a high level of gas temperature in front of the turbine of the bypass turbojet in comparison with the straight turbojet and also the appearance of pumping in the first stage compressor.

3. The throttling of the bypass turbojet is connected with the redistribution of full thrust between the stages — the relative growth of its component in the second stage. Thus, the work regime of the bypass turbojet continuously deviates from the optimum.

4. The relative rise in the temperature of the gas in front of the turbine and in the degree of compression in the second stage compressor leads in practice to continuous deterioration in efficiency when throttling the bypass turbojet.

5. Raising the speed and height of flight improves the throttling characteristics of the bypass turbojet, broadening the range of reliable functioning of the engine.

6. The most rational control program for the single-shaft bypass turbojet on the stand and in flight is that of $f_5^I = \underline{c}$ and $f_5^{II} = \underline{c}$.

7. A comparison of the three control programs for the bypass

turbojet shows that they have an insubstantial influence on its efficiency, for example, when $\bar{R} = 0.7$ the examined methods of control give fluctuations in specific fuel consumption of not more than 10%.

8. Improving the operating characteristics of the bypass turbojet in starting, accelerating, and cruising work regimes requires the the use of more effective measures of controlling the engine than by control of the first stage jet nozzle of the turbojet. One of these methods is the use of a double-shaft arrangement for the bypass turbojet; another is the exclusion of the second stage from work in lowered regimes, i.e., transition from bypass turbojet to straight turbojet; finally, a third is the use of reversible vanes in the compressor.

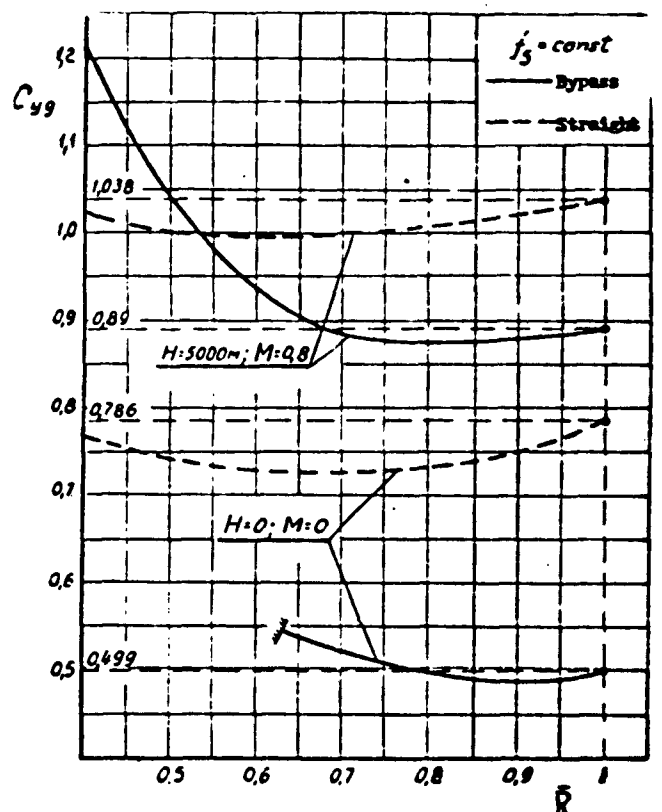

Fig. 13. Comparison of specific fule consumption in bypass and straight turbojets when throttled on stand and in flight.

REFERENCES

1. A. L. Klyachkin. The Theory of Bypass Air-Breathing Engines. RKVIAVU, Riga, 1959.

2. L. S. Dmitriyev. Fundamentals of Combustion Theory. RKVIAVU, Riga, 1958.

Department of Aviation Engine Theory

Received October 23, 1961

DISTRIBUTION LIST

DEPARTMENT OF DEFENSE	Nr. Copies
HEADQUARTERS USAF	
AFCIN-3D2	1
ARL (ARB)	1
OTHER AGENCIES	
CIA	1
NSA	6
DIA	9
AID	2
OTS	2
AEC	2
PWS	1
NASA	1
ARMY	3
NAVY	3
RAND	1

MAJOR AIR COMMANDS	Nr. Copies
AFSC	
SCFDD	1
ASTIA	25
TDHTL	5
TDBDP	5
AEDC (AEY)	1
SSD (SSF)	2
BSD (BSF)	1
AFFTC (FTY)	1
AFSWC (SWF)	1